# Predicting twin boundaries in molecular crystals using evolutionary algorithm: Application to aspirin, RDX, and HMX

Chi Ren [1,*] Hairui Ding [1,*] Artem R. Oganov [2] Zhaonan Wang,[1] Haixu Cui,[3,†] Huajie Song,[4,‡] and Xiao Dong [1,§]

[1]*Key Laboratory of Weak-Light Nonlinear Photonics and School of Physics, Nankai University, Tianjin 300071, China*

[2]*Skolkovo Institute of Science and Technology, Moscow 121205, Russia*

[3]*College of Physics and Materials Science, Tianjin Normal University, Tianjin 300387, China*

[4]*Institute of Applied Physics and Computational Mathematics, Beijing 100088, China*

(Received 15 December 2025; revised 16 March 2026; accepted 24 March 2026; published 13 April 2026)

Research on twin boundaries (TBs) in molecular crystals has primarily emphasized their effect on mechanical properties and applications, with limited focus on microstructural details. Twin identification typically relies on extensive experiments, lacking reliable computational predictions. Here, we extend to molecular crystals the previously developed evolutionary methodology for predicting grain boundary structures in atomic crystals. To achieve that, care must be taken of molecular orientations, conformations, and grain displacements during global optimization. We apply this method to predict possible TBs on the (100), (010), and (001) planes of polymorph I of aspirin; the (100), (010), (001), (102), (110), and (210) planes of $\alpha$-RDX; and the (010), (10$\bar{1}$), (011), (101), and (110) planes of $\beta$-HMX. For HMX, the lowest-energy (101) TB matches experimentally reported twin, validating our approach. We predict unexpected low-energy TB configurations, including a unique cluster-like structure on (100) plane of aspirin and numerous conformational changes in RDX. Finally, we discuss the characteristics and patterns of molecular crystal twin formation.

DOI: 10.1103/7cdh-875w

## I. INTRODUCTION

The microscopic deformation of crystals is primarily accommodated by dislocation-mediated slip and mechanical twinning via atomic shear (deformation twinning). Twinning, defined as symmetric intergrowth of two or more crystals, can also occur during crystal growth (growth twinning) and phase transitions (transformation twinning), and is an extremely common phenomenon. The interface between crystals forming a twin structure is termed a twin boundary (TB). While TBs in simple atomic crystals have been extensively studied [1–3], research on TBs in molecular crystals has predominantly focused on how they impact the mechanical properties and applications of materials [4,5], with less attention to their atomic-scale structure. Usually, the twinning law corresponds to the missing symmetry element of the point group of the crystal; the twin effectively restores this symmetry. Consequently, twinning is expected to be more prevalent in low-symmetry crystals [6].

Early twinning models were largely based on the coincident site lattice (CSL) theory [7,8], which evaluates the propensity for twinning by quantifying the lattice coincidence between adjacent grains. While effective for single-element crystals, this model, being based solely on lattice geometry and symmetry, is insufficient for multicomponent atomic and molecular crystals, where specific bonding interactions are critical. Subsequently, the $\gamma$-surface method was developed to predict twin structures in molecular crystals [9], overcoming some of the limitations of the CSL theory by incorporating bonding relationships and offering greater predictive flexibility. However, in molecular crystals, the lattice sites are occupied by molecules possessing internal degrees of freedom and specific geometries, rather than simple points as in atomic crystals. This distinction can induce molecular reorientation and conformational changes at the boundary to minimize the TB energy. Furthermore, studies indicate that grain boundaries (GBs) may exist as ensembles of multiple low-energy metastable configurations rather than a single structure [9–11], underscoring the need for more robust GB prediction methods. Recently, various heuristic algorithms have been successfully applied to predict diverse crystal structures [12–14]. Among these, evolutionary algorithms, inspired by evolutionary biology, have been implemented in the USPEX code [14]. USPEX has successfully predicted structures for bulk crystals [14], 2D materials [15], surfaces [16], and polymers [17]. Building on this, Zhu *et al.* extended USPEX to predict GBs in atomic crystals [18]. In the present work, we further extend this approach to develop a method for predicting GB structures in molecular crystals, thereby addressing the challenges outlined above. We demonstrate this method by predicting the TBs for the habit planes of aspirin, hexahydro-1,3,5-trinitro-1,3,5-triazine (RDX), and octahydro-1,3,5,7-tetranitro-1,3,5,7-tetrazocine (HMX).

Aspirin crystals are built up by a combination of hydrogen bonds and van der Waals forces, resulting in stronger cohesion compared to RDX and HMX crystals, which are

*These authors contributed equally to this work.
†Contact author: hxcui@tjnu.edu.cn
‡Contact author: song_huajie@iapcm.ac.cn
§Contact author: xiao.dong@nankai.edu.cn

 

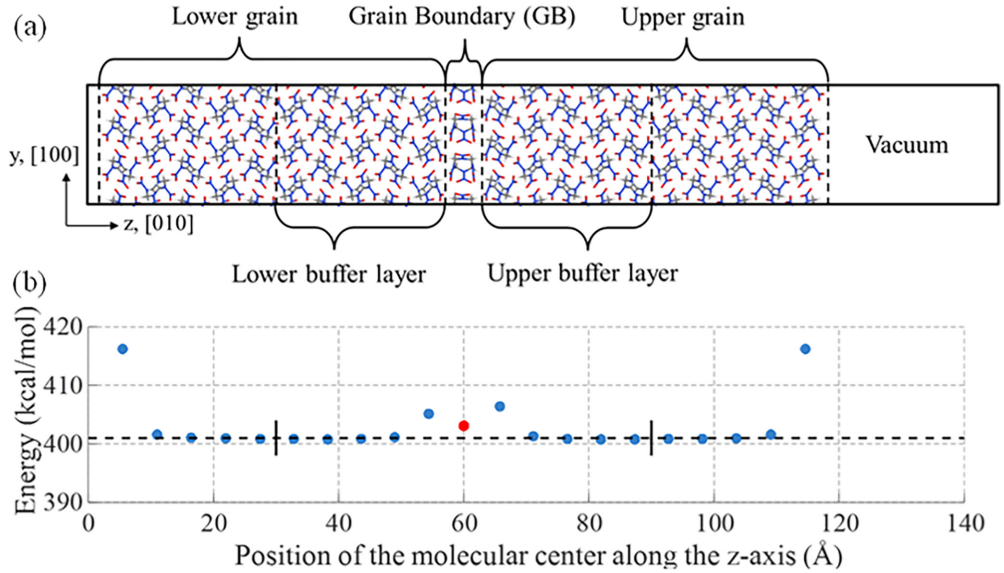


FIG. 1. (a) Representation of the TB structure, using a predicted HMX (010) TB as an example. The model comprises upper grain, lower grain, and GB in between. During optimization, buffer layers (from each grain) and the GB are relaxed via MD simulation. (b) Potential energy statistics of molecules at different positions along the z-axis. The horizontal axis scale corresponds to the model in (a). The red dots in the figure represent the potential energy of molecules in the GB, while the blue dots represent the rest.

built up solely by van der Waals interactions. Consequently, aspirin exhibits more pronounced fracture behavior under stress. Early computational studies identified the (100) plane as having the weakest interfacial interactions in aspirin, followed by the (001) face [19]. Subsequent nanoindentation experiments confirmed that plastic flow occurs more readily on the (100) plane, while the (001) face demonstrates significantly lower fracture toughness, establishing it as the preferred cleavage plane [20]. Furthermore, aspirin is known for its polymorphism and tendency to form polymorphic intergrowths [21]. This study employs the most stable form I of aspirin, with the (100), (010), and (001) planes selected as symmetric faces for twin construction and TB structure prediction. In contrast, RDX and HMX are well-known high energy density materials, and defects within these crystals can act as hot spots under external stimuli, potentially leading to detonation. Research on RDX defect has primarily focused on dislocations and slip systems, with the (010) plane identified as the primary slip plane [22]. Secondary slip systems are also active on the (001), (011), (021), and $(02\bar{1})$ faces [22–24]. Recent studies of RDX under shock loading have revealed nanoscale shear bands, with localized twin strain bands observed as transient microstructures during band formation [25], suggesting the possibility of twinning in RDX. For HMX, numerous experimental studies have documented widespread twinning [26,27], characterized by the twin elements: $K_1 = (101)$, $\eta_2 = [10\bar{1}]$, $K_2 = (10\bar{1})$, $\eta_2 = [101]$ [28]. Under stress, twin formation in HMX is associated with specific slip systems on the (101) planes. Simulations indicate that HMX accommodates strain via slip, where, under certain conditions, functional group and molecular rotations facilitate structural reconstruction, providing a mechanism for twinning [28]. In this study, the most stable phases of RDX ($\alpha$) and HMX ($\beta$) under normal conditions were selected. TB searches were conducted on the (001), (010), (100), (102), (110), and (210) planes of $\alpha$-RDX and the (010), $(10\bar{1})$, (011), (101), and (110) planes of $\beta$-HMX.

Although experimental studies have demonstrated the existence of twinning in HMX and presented morphological images, these images do not provide atomic-level structural information, and the specific TB structure remains controversial [28]. Similarly, the twin bands in RDX, which serve as transient precursors to shear bands, are not well understood. By predicting TBs for molecular crystals with both known (HMX) and unconfirmed (aspirin, RDX) twinning behavior, we aim to validate existing models and predict new twins and metastable configurations. Analyzing the common features of low-energy TBs may provide critical insights into the mechanisms of twin formation.

## II. METHODOLOGY

### A. Evolutionary search

Although this study focuses on TBs in molecular crystals, the developed method is applicable to general GBs. Herein, "GB" refers to the region predicted by the evolutionary algorithm, which includes the TB we study. The model representation of GBs is shown in Fig. 1(a), where the model is divided into three parts: the upper crystal grain, the lower crystal grain, and the GB region. The GB region is fully variational, i.e., the number, positions, and orientations of molecules are determined by global optimization. Crystal grain regions correspond to the fixed structure of the bulk crystal, except that portions of the upper and lower grains adjacent to the GB are treated as buffer layers, i.e., are allowed to relax together with the GB region via molecular dynamics (MD) simulation. In this work, the thickness of the crystal grain along the $z$ axis is 60 Å, of which the buffer layer is 30 Å thick, and the GB layer thickness is one molecular

layer, as referenced by the horizontal axis scale in Fig. 1(b). A population of GB structures, initiated using random structure generators, evolves iteratively via variational operators (heredity and mutations) and selection of the fittest within the population.

Our method for predicting molecular crystal GBs at 0 K improves and extends the USPEX-based approach for GBs of atomic crystals developed by Zhu *et al.* [18]. The principal modification involves using molecules, rather than atoms, as the fundamental building units during the evolutionary search, with structure generation accounting for molecular symmetry. To address the complexity of molecular crystals and expand the search space, the methodology incorporates concepts from $\gamma$-surface calculations by permitting relative displacements of the upper and lower grains parallel to the twin plane. Furthermore, the cross-sectional area of the GB is allowed to undergo supercell expansion, with a maximum expansion factor of 6 (considering all integer $n \times m$ configurations satisfying $n \cdot m \leqslant 6$) to sample a wider range of possible GB structures. Furthermore, specific minimum spacings for atoms and molecular centers were set for different molecular systems.

The evolutionary process, including heredity and mutation operators, follows the standard USPEX code [14,29]. For this work, the population size was set to 50 structures per generation. After energy evaluation, the lowest-energy 60% of the population were allowed to produce offspring. The next generation included 15% lowest-energy structures transferred from the previous generation, 30% obtained via heredity (combining segments from two parent structures), 30% via random mutation (altering molecular density and generating symmetry-adapted GBs), 30% via softmutation (using soft phonon modes to drive structural transitions), and 10% via orientation mutation that adjusts molecular orientations within the GB to better match the adjacent grains and maximize coherence of the GB. Global optimization on the high-dimensional energy landscape of molecular crystals is a difficult problem, and to ensure reliable results, evolutionary searches were conducted for 100 generations.

### B. Structure relaxation and energy evaluation

Structure relaxations and energy calculations were done using the LAMMPS code [30]. Periodic boundary conditions were applied in all directions; the inclusion of a 30 Å vacuum layer perpendicular to the GB in the model was sufficient to isolate interactions between the periodic images of the upper and lower grains. To stabilize the GB configuration, a 10 ps MD simulation was conducted for the GB and buffer layers. The conjugate gradients method was used to minimize the system's potential energy and stress both before and after the MD simulation. MD simulations were performed in the *NVT* ensemble at 300 K, using the Nosé-Hoover thermostat. This entire procedure—comprising energy minimization, MD simulation, and a final minimization—was performed three times sequentially, with progressively stricter convergence criteria for the minimizations.

For the three molecular crystals studied, the unit cell parameters are as follows. Form I aspirin: $a = 11.430$ Å, $b = 6.591$ Å, $c = 11.395$ Å, and $\beta = 95.68^\circ$ [31]. For aspirin, we used the tailor-made force field developed by Chen and Neumann [31], which provides high energy accuracy for precise energy ranking and has demonstrated excellent performance in crystal structure prediction. $\alpha$-RDX: $a = 13.131$ Å, $b = 11.379$ Å, and $c = 10.569$ Å. $\beta$-HMX: $a = 6.371$ Å, $b = 10.987$ Å, and $c = 7.345$ Å, $\beta = 102.62^\circ$. It is important to note that these unit cells serve only as the basis for constructing the initial upper and lower grains; the specific GB model must be adapted according to the twin plane being investigated. For RDX and HMX, we used the all-atom flexible force field developed by Smith and Bharadwaj [32], with modifications for TB prediction. This force field has been extensively validated in numerous computational studies of HMX and RDX [28,33,34], confirming its reliability.

### C. Analysis of the results

As the evolutionary search proceeds, it tends to converge within a narrow energy range, producing similar TB structures. To obtain a comprehensive understanding of TBs and metastable configurations in molecular crystals, we do not select structures based solely on energy ranking. Because the evolutionary algorithm includes heredity operations, GBs with similar volumes are prone to having identical or highly similar structures. Therefore we classify the searched structures based on their GB volume and then perform energy ranking within each category. This approach allows for the selection of the five lowest-energy TBs with distinct structures for each crystal plane.

We calculate the interface energy (here called the GB energy) as the energy change per area induced by the boundary. As illustrated in Fig. 1(b), the red dots represent molecules within the GB region, while the blue region represents the rest. It is important to note that the presence of a GB often increases the potential energy of molecules beyond the immediate boundary layer. Consequently, we calculate the GB energy using the following formula:

$$\gamma_{gb} = (E_{gb} - NE_m)/A.$$

Here, $E_{gb}$ is the total molecular potential energy within the spatial range where the GB induces an energy increase [demarcated by the black solid line in Fig. 1(b)], $N$ is the number of molecules within this range, $E_m$ is the average energy per molecule in a perfect bulk crystal [indicated by the black dashed line in Fig. 1(b)], and $A$ is the area of the twin plane. It is $\gamma_{gb}$ that we use as a measure of the fitness of each GB model.

## III. RESULTS AND DISCUSSION

### A. The search for aspirin TB structures

For form I aspirin, we selected the (100), (010), and (001) planes as twin planes to predict their corresponding TB structures. Figure 2(a) presents six representative low-energy structures, selected to include all searched crystal planes and ranked by their GB energy. The lowest-energy structure, found on the (100) plane, has a GB energy of $\gamma_{\mathrm{gb}} = 0.02\ \mathrm{J/m^2}$—an order of magnitude lower than other aspirin TBs. This structure induces minimal molecular changes in the buffer layers. However, molecules within the TB region

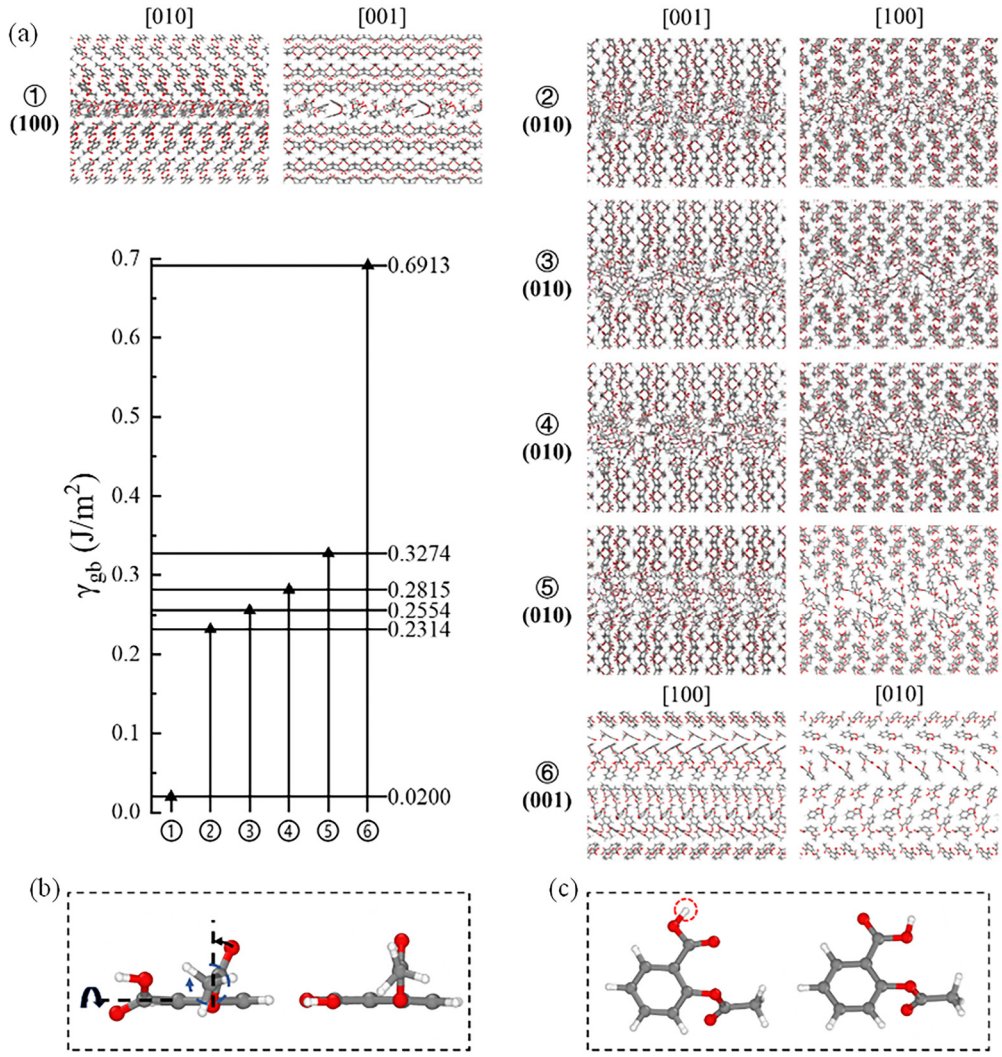


FIG. 2. (a) Energy ranking of low-energy TBs predicted for aspirin, with corresponding structural models. (Gray: C; red: O; white: H.) [(b) and (c)] Molecular conformational changes within the TBs. For each pair, the left panel shows the changed conformation with key alterations highlighted, and the right panel shows the molecule in the perfect crystal.

itself exhibit multiple orientations, and some aspirin molecules undergo simple conformational changes. These changes include a twist of the bond between the carboxyl group and the benzene ring, disrupting the coplanarity of the system, and angular shifts in the acetyl group, collectively resulting in the molecular structure shown in Fig. 2(b). These torsional changes are not necessarily concurrent or identical in magnitude. Furthermore, as shown in Fig. 2(c), some aspirin molecules within the TB adopt a conformation where the carboxyl hydrogen is oriented away from the acetyl group, matching the molecular geometry reported for form IV aspirin crystals [35]. This observation, which also occurs in other TBs, suggests that the carboxyl and acetyl groups possess relatively high conformational flexibility within the molecular framework. Structures ②—④, influenced by the allowed relative grain displacements during the search, resemble a reconstruction towards a bulk-like configuration. However, due to the mirror symmetry relationship between the upper and lower grains, a perfect crystal cannot be reconstituted, resulting in these distinct, yet energetically similar, interfacial structures. Although structure ⑤ does not exhibit such reorganization, it induces significant molecular changes in the buffer layers, leading to a higher GB energy. Structure ⑥ represents the lowest-energy TB predicted for the (001) plane. In this configuration, the orientation of multiple molecular layers is altered, a phenomenon frequently observed in our predictions for aspirin, which we attribute to a potential relationship with the known propensity of aspirin to polymorphic intergrowth [21].

In summary, for the twin systems constructed for form I aspirin, the (100) plane is the most favorable for twinning. The low-energy TB structure ①, when viewed along the [010] direction, exhibits a local, cluster-like molecular arrangement. As discussed in reference [9], such dense packing may represent a balance between symmetry, packing forces, and surface tension, suggesting that molecular aggregates at nucleation sites in aspirin might not adopt the structure of the bulk crystal. This is consistent with reported weak interlayer interactions between (100) planes [19], suggesting that TB molecules are subject to weaker lattice constraints. In

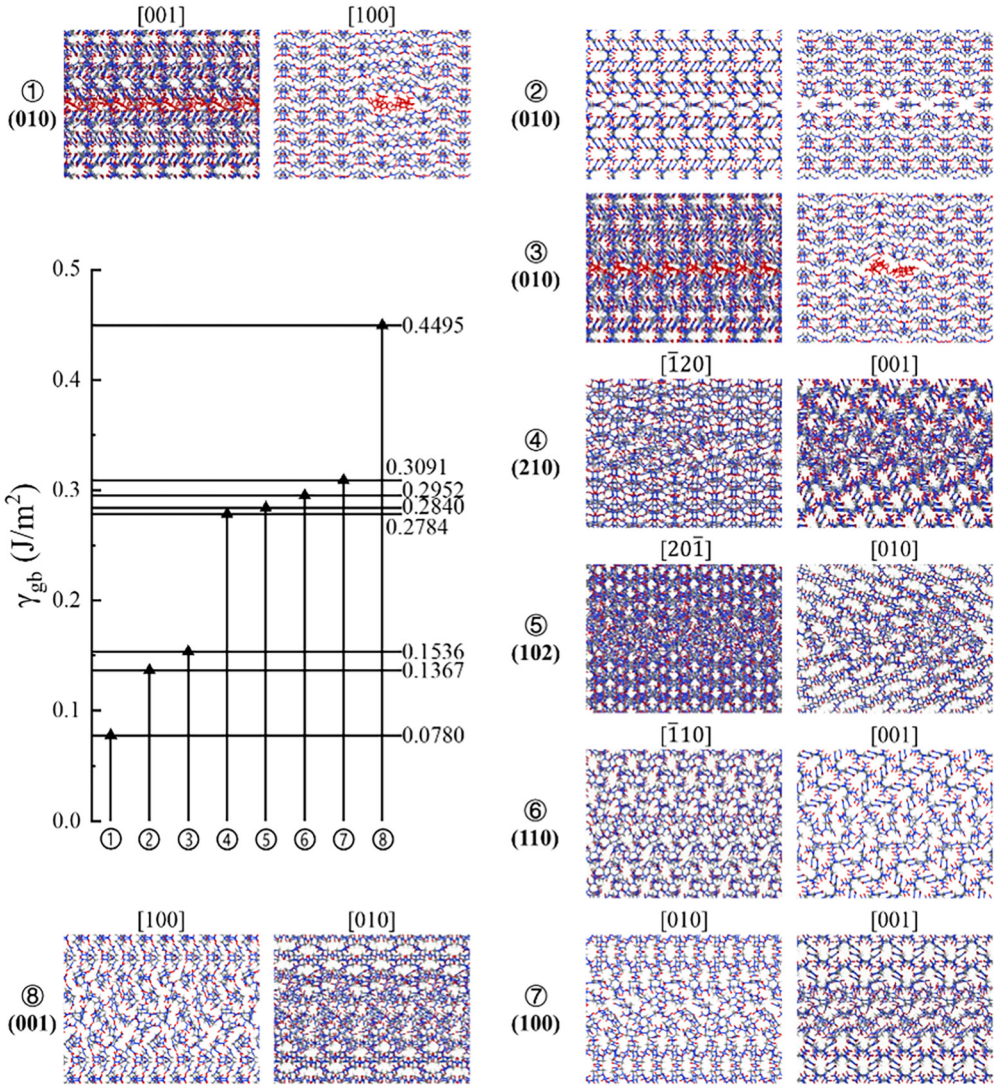


FIG. 3. Energy ranking of low-energy TBs predicted for RDX, with corresponding structural models. (Blue: N; gray: C; red: O; white: H.) Red molecules in ① and ③ represent the GB molecules.

contrast, the strong interlayer interactions between adjacent (010) planes [19] explain why searches on this plane yielded structures that resemble reorganized perfect interfaces rather than genuine low-energy TBs. Although the (001) plane also exhibits weak interface interactions [19], no low-energy TB was identified. This may be related to its low fracture toughness [20], as our search yielded multiple separated interfaces that were discarded.

### B. The search for RDX TB structures

For $\alpha$-RDX, we selected the (100), (010), (001), (102), (110), and (210) planes as twin planes to predict their corresponding TB structures. Figure 3 presents the eight lowest-energy structures identified, selected to ensure coverage of all searched planes and ranked by their GB energy. The three lowest-energy structures all originate from the (010) plane. Had the selection not required representation from all planes, more low-energy structures from the (010) plane would have been included, a finding consistent with its identification as the primary slip plane possessing weak interlayer interactions [22,24]. However, among these three lowest-energy structures, configurations ① and ③ more closely resemble point defects within an otherwise perfect crystal. In Fig. 3, the GB molecules in ① and ③ are highlighted in red. The projection along the [100] direction shows that only the few molecules highlighted in red originate directly from the evolutionary search, whereas other molecules in the same layer likely were pulled from the buffer layers during MD relaxation, forming a more compact structure. These configurations are not the intended twin structures, whereas structure ② aligns with our objective. In ②, the upper and lower grains exhibit an approximate mirror symmetry about the (010) plane. Molecules at the interface change conformation and orientation, with adjacent molecules adopting opposite orientations to form a sequentially arranged, nearly mirror-symmetrical structure when viewed in projection. This TB structure appears to effectively balance the interactions

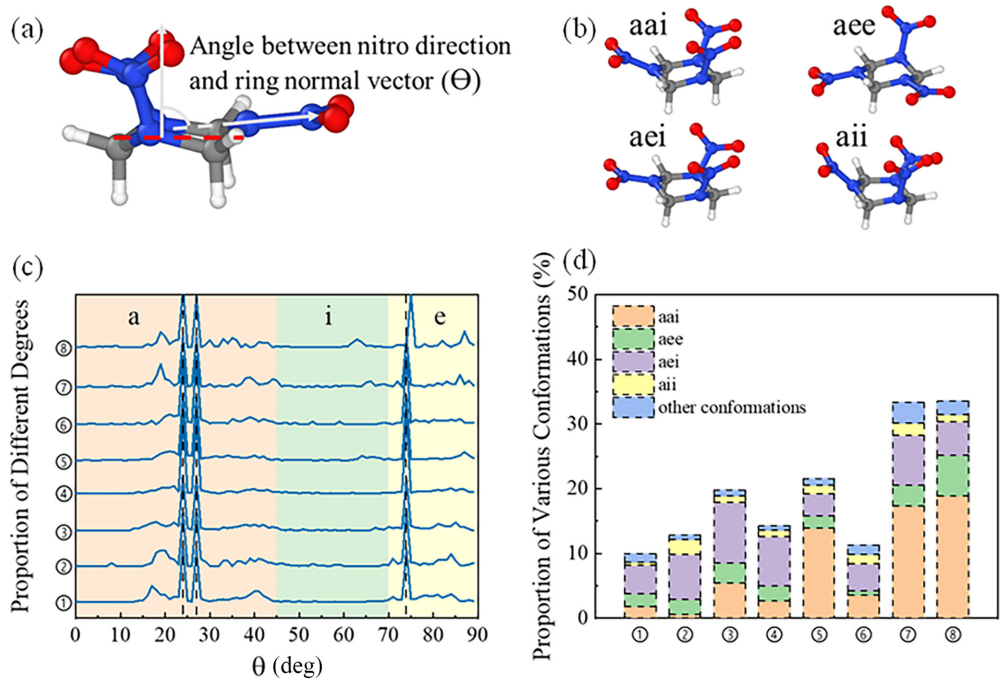


FIG. 4. Analysis of molecular conformations in RDX twins. (a) Definition of the angle $\theta$ (0 ° to 90 °). (b) Primary non-Caae conformations found in the twins. (c) Statistical distribution of $\theta$ for molecules in the eight low-energy structures, normalized by molecule count; background color indicates the nitro conformation type. The three black vertical dashed lines represent $\theta$ values in the perfect crystal. (d) Stacked bar chart showing the proportions of different molecular conformations (excluding Caae).

between the adjacent grains. In higher-energy structures (④ onwards), changes in molecular orientation and conformation become more pronounced.

To further elucidate the predicted TB structures of RDX, we performed a statistical analysis of molecular conformations. RDX molecules can adopt chair (C), twist (T), or boat (B) ring conformations, with chair (C) being the most stable at standard conditions [25]. The angle between the nitro group and the normal to the central ring further classifies the nitro group's conformation into three types: when the angle is close to 90 °, it is referred to as the pseudo-equatorial (e) conformation, when the angle is less than 45 °, it is referred to as the axial (a) conformation, and those between these two angles are marked as intermediate (i) [25,34]. The prevalent conformation in $\alpha$-RDX is Caae [33,36]. We determined the ring plane normal via principal component analysis and the nitro group direction from the N-N bond vector, calculating the angle $\theta$ as defined in Fig. 4(a). This method was applied to statistically analyze the distribution of $\theta$ and the proportion of non-Caae conformations in the eight low-energy structures [Figs. 4(c) and 4(d)], with major alternative conformations shown in Fig. 4(b). Even in these low-energy TB candidates, the nitro group angle $\theta$ deviated from the perfect crystal value to accommodate the boundary. The conformational statistics reveal that at least 10% of molecules underwent changes (Structure ①). Conformations such as aai, aee, aei, and aii, primarily observed in buffer layer molecules adapting to the TB, were identified. Structures ① and ③ show high-symmetry aaa and eee conformations at the point defect sites, which are uncommon in $\alpha$-RDX [25]. Structure ② exhibits only the aee conformation at the GB, typically generated from the aae conformation under mechanical strain. The aae-to-aee transition has a low energy barrier, occurring readily without disrupting the stability of the crystal [33].

In summary, among the RDX TB search results, structures ① and ③ are point defect-like, closely resembling the perfect crystal outside the defect core, which results in their low GB energy. In contrast, structure ② features a relatively stable Caee conformation and an ordered arrangement in the TB, albeit still inducing changes in the buffer layers. Most higher-energy structures exhibit more severe buffer layer distortions. Although structure ⑥ has a lower proportion of conformational changes, its higher GB energy suggests that the energy penalty originates predominantly from unfavorable interfacial interactions rather than molecular distortions. The prevalence of high-energy RDX conformations in these interfaces also indicates that RDX may not readily form stable twin structures.

### C. The search for HMX TB structures

For $\beta$-HMX, TB structures were predicted for the (010), (10$\bar{1}$), (011), (101), and (110) planes. Figure 5 presents the eight lowest-energy structures selected from this search. As the only molecular crystal in this study with experimentally confirmed twinning, HMX exhibits twin structures where the molecular arrangement shows no buffer layer changes. With the exception of structure ⑧ (where a set of nitro groups on opposite sides orient in the same direction) no conformational changes occur in the TB molecules, with only minor orientational adjustments observed. These features indicate that the TB serves as a structurally coherent transition between the upper and lower grains. The lowest-energy twin structure is predicted for the (101) twin plane. In this case, the TB structure matches that of a perfect crystal. When viewed along the

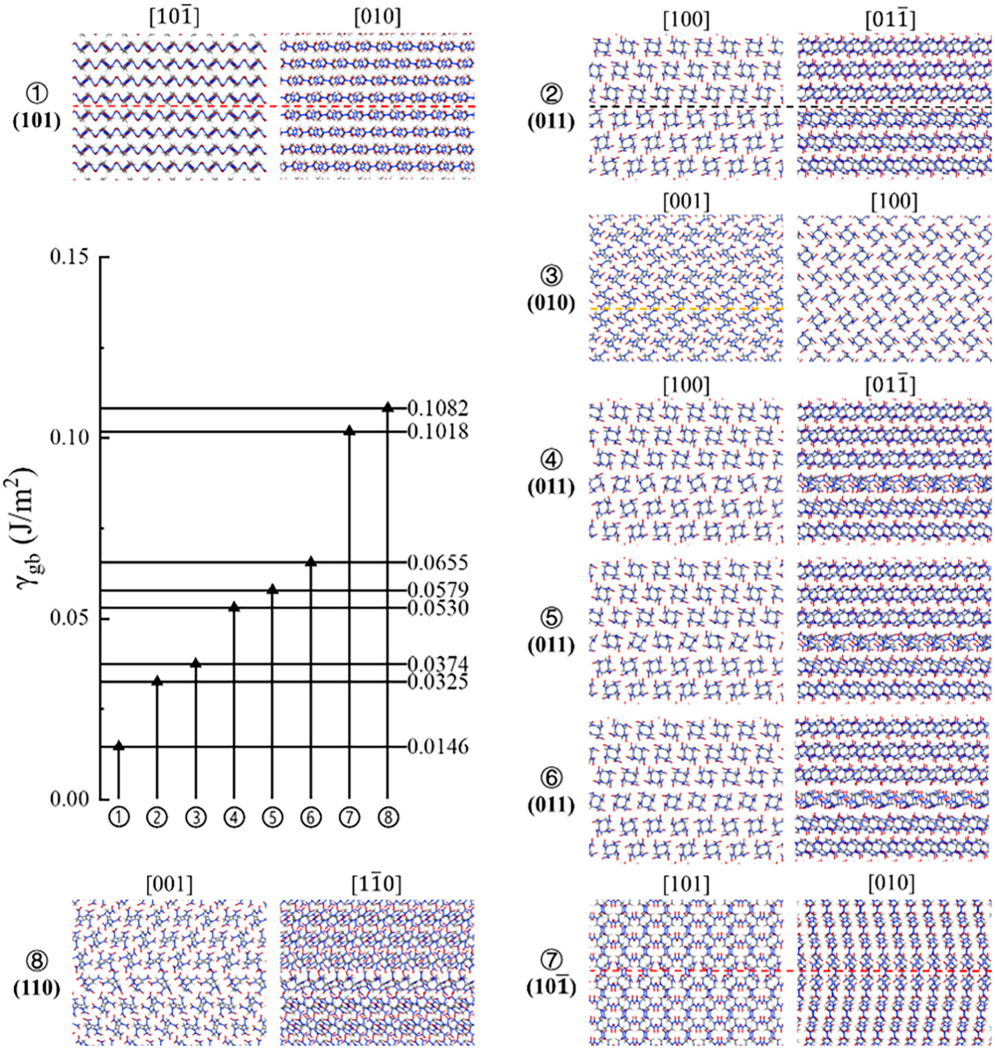


FIG. 5. Energy ranking of low-energy TBs predicted for HMX, with corresponding structural models. (Blue: N; gray: C; red: O; white: H.) Different colored dashed lines are used to indicate the boundaries of different features.

[10$\bar{1}$] direction, the twin reconstructs the perfect crystal structure. However, the projection along the [010] direction reveals mirror symmetry, with the [10$\bar{1}$] crystal direction acting as the symmetry axis (red dashed line in Fig. 5①). This apparent perfection along [10$\bar{1}$] arises from a 1/2-unit cell displacement between the upper and lower grains along the [010] direction in the actual 3D structure. This predicted structure is consistent with the reported twin elements for HMX: $K_1$ =(101), $\eta_2$ = [10$\bar{1}$], $K_2$ =(10$\bar{1}$), $\eta_2$ = [101] [28]. A similar structure is found in TB structure ⑦, constructed from the (10$\bar{1}$) plane. Its projection along one direction approximates a perfect crystal, while another projection shows mirror symmetry (red dashed line in Fig. 5⑦). Slight local morphological deviations from the perfect crystal likely account for its higher GB energy. Structures ② and ③ also exhibit relatively low GB energies, with their TB regions reconstructing the perfect crystal structure. Structure ② resembles broken mirror symmetry due to a relative displacement between the grains, with the black dashed line in the figure representing its boundary. Structure ③ lacks a mirror axis and is more akin to a stacking fault on the lower grain, characterized by different molecular layer connections at the TB/lower-grain interface (orange dashed line in Fig. 5③). Structures ④–⑥ show similar characteristics, where the TB layers form distinct structures as transitions between grains. Compared to the near-perfect reconstruction in structure ② from the same plane, their higher GB energy is expected. Structure ⑧ presents a similar case, with the additional feature of a conformational change in the HMX molecule.

Our simulations predict that the (101) plane readily forms a twin structure in $\beta$-HMX. This structure is not a simple mirror image across the twin plane but involves a 1/2-unit cell displacement along [010], consistent with reported structures [28]. Furthermore, the asymmetric TB on the (011) plane (structure ②) also possesses a low GB energy. Structure ⑦, which shares the same twinning mode as ①, shows slight local molecular angle variations, leading to a higher energy. Given the high consistency of structure ⑦ with the known HMX twin mode, we propose that the GB structures ② and ⑦ could represent previously unidentified stable TBs in HMX crystals.

## IV. CONCLUSION

In this work, we developed an evolutionary algorithm for predicting GB structures in molecular crystals, extending the approach established by Zhu *et al.* for atomic crystals [18]. The method incorporates concepts from the $\gamma$-surface approach to allow relative displacements between grains. The GB region is treated as a twin transition zone and is optimized using MD. Applied to aspirin, RDX, and HMX, the method successfully predicts TBs on their respective habit planes, identifying the most probable twinning planes and atomic structures. For $\beta$-HMX, the lowest-energy TB identified on the (101) plane matches previously reported experimental and computational twin structures [27,28], thereby validating our approach.

For aspirin, the (100) plane yields a stable, cluster-like TB ($\gamma_{gb} = 0.02\ J/m^2$) with varied molecular conformations, potentially resembling nucleation sites. The observed conformational changes in aspirin primarily involve twisting of the carboxyl group, shifts in the acetyl group angle, and repositioning of the carboxyl hydrogen. In contrast, RDX exhibits unstable conformations across its layers; only the ordered Caee conformations found in the TB on the (010) plane show potential stability, although they compete with lower-energy point defects. For HMX, the low-energy TBs restore the perfect crystal structure without inducing changes in the buffer layers. The (101) mirror twin is the dominant configuration, while a similar twinning mode observed on the $(10\bar{1})$ plane and the relatively low GB energy found on the (011) plane suggest the existence of additional, so far undiscovered modes of twinning.

In general, twin formation in molecular crystals is associated with near-perfect reconstructions at the interface to minimize energy, a process governed by local symmetry. However, in systems such as aspirin and RDX, the very limited number of low-energy, bulk-like TB configurations enables the formation of complex twins, highlighting the significant role of molecular flexibility. This method provides a predictive tool for defect engineering in molecular crystals.

## ACKNOWLEDGMENTS

This work was supported by the 2020-JCJQ project (Grant No. GFJQ2126-007), the NSFC (Grants No. 92263101, No. 12574019, and No. 12174200), Academy for Advanced Interdisciplinary Studies, Nankai University (Grants No. 9261500174 and No. 9261500166), the Doctor Foundation of Tianjin Normal University (Grant No. 52XB1911), and the Tianjin Education Commission Research plan (Grant No. 2021KJ181). The calculations were performed and supported by Tianhe II in Guangzhou and the Supercomputing Center of Nankai University (NKSC). A.R.O. acknowledges support from the Russian Science Foundation (Grant No. 24–43-00162).

## DATA AVAILABILITY

The data that support the findings of this article are openly available [37,38].

[1] K. Tong, X. Zhang, Z. H. Li, Y. B. Wang, K. Luo, C. M. Li, T. Y. Jin, Y. Q. Chang, S. Zhao, Y. J. Wu, *et al.*, Structural transition and migration of incoherent twin boundary in diamond, Nature (London) **626**, 79 (2024).

[2] J. W. Xiao, B. Wen, B. Xu, X. Y. Zhang, Y. B. Wang, and Y. J. Tian, Intersectional nanotwinned diamond-the hardest polycrystalline diamond by design, npj Comput. Mater. **6**, 119 (2020).

[3] T. Frolov, W. Setyawan, R. J. Kurtz, J. Marian, A. R. Oganov, R. E. Rudd, and Q. Zhu, Grain boundary phases in bcc metals, Nanoscale **10**, 8253 (2018).

[4] M. B. Al-Handawi, P. Commins, A. S. Dalaq, P. A. Santos-Florez, S. Polavaram, P. Didier, D. P. Karothu, Q. Zhu, M. Daqaq, L. Li, *et al.*, Ferroelastic ionic organic crystals that self-heal to 95%, Nat. Commun. **15**, 8095 (2024).

[5] T. Sasaki, Mechanical twinning in organic crystals, CrystEngComm **24**, 2527 (2022).

[6] S. Parsons, Introduction to twinning, Acta Cryst. D **59**, 1995 (2003).

[7] D. H. Warrington, The coincidence site lattice (CSL) and grain boundary (DCS) dislocations for the hexagonal lattice, J. Phys. Colloq. **36**, C4 (1975).

[8] R. W. Balluffi, A. Brokman, and A. H. King, CSL/DSC lattice model for general crystalcrystal boundaries and their line defects, Acta Metall. **30**, 1453 (1982).

[9] H. F. Lieberman, L. Williams, R. J. Davey, and R. G. Pritchard, Molecular configuration at the solid-solid interface: Twinning in saccharin crystals, J. Am. Chem. Soc. **120**, 686 (1998).

[10] A. Hill, W. Kras, F. Theodosiou, M. Wanat, D. Lee, and A. J. Cruz-Cabeza, Polymorphic solid solutions in molecular crystals: Tips, tricks, and switches, J. Am. Chem. Soc. **145**, 20562 (2023).

[11] A. D. Bond, Polymorphism in molecular crystals, Curr. Opin. Solid State Mater. Sci. **13**, 91 (2009).

[12] Y. C. Wang, J. Lv, L. Zhu, and Y. M. Ma, Crystal structure prediction via particle-swarm optimization, Phys. Rev. B **82**, 094116 (2010).

[13] C. J. Pickard and R. J. Needs, *Ab initio* random structure searching, J. Phys.: Condens. Matter **23**, 053201 (2011).

[14] A. R. Oganov and C. W. Glass, Crystal structure prediction using *ab initio* evolutionary techniques: Principles and applications, J. Chem. Phys. **124**, 244704 (2006).

[15] X. F. Zhou, X. Dong, A. R. Oganov, Q. Zhu, Y. J. Tian, and H. T. Wang, Semimetallic two-dimensional boron allotrope with massless Dirac fermions, Phys. Rev. Lett. **112**, 085502 (2014).

[16] Q. Zhu, L. Li, A. R. Oganov, and P. B. Allen, Evolutionary method for predicting surface reconstructions with variable stoichiometry, Phys. Rev. B **87**, 195317 (2013).

[17] Q. Zhu, V. Sharma, A. R. Oganov, and R. Ramprasad, Predicting polymeric crystal structures by evolutionary algorithms, J. Chem. Phys. **141**, 154102 (2014).

[18] Q. Zhu, A. Samanta, B. X. Li, R. E. Rudd, and T. Frolov, Predicting phase behavior of grain boundaries with evolutionary search and machine learning, Nat. Commun. **9**, 467 (2018).

[19] H. Umeyama, S. Nakagawa, and I. Moriguchi, Molecular orbital study of the cleavage of aspirin crystals, J. Phys. Chem. **83**, 2048 (1979).
[20] D. Olusanmi, K. J. Roberts, M. Ghadiri, and Y. Ding, The breakage behaviour of Aspirin under quasi-static indentation and single particle impact loading: Effect of crystallographic anisotropy, Int. J. Pharm. **411**, 49 (2011).
[21] A. D. Bond, R. Boese, and G. R. Desiraju, On the polymorphism of aspirin: Crystalline aspirin as intergrowths of two "polymorphic" domains, Angew. Chem. Int. Ed. **46**, 618 (2007).
[22] P. J. Halfpenny, K. J. Roberts, and J. N. Sherwood, Dislocations in energetic materials: Part 3 Etching and microhardness studies of pentaerythritol tetranitrate and cyclotrimethylenetrinitramine, J. Mater. Sci. **19**, 1629 (1984).
[23] H. G. Gallagher, P. J. Halfpenny, J. C. Miller, and J. N. Sherwood, Dislocation slip systems in pentaerythritol tetranitrate (PETN) and cyclotrimethylene trinitramine (RDX), Phil. Trans. R. Soc. Lond. A **339**, 293 (1992).
[24] N. Mathew, C. R. Picu, and P. W. Chung, Peierls stress of dislocations in molecular crystal cyclotrimethylene trinitramine, J. Phys. Chem. A **117**, 5326 (2013).
[25] S. Izvekov and B. M. Rice, Microscopic mechanism of nanoscale shear bands in an energetic molecular crystal ($\alpha$-RDX): A first-order structural phase transition, Phys. Rev. B **106**, 104109 (2022).
[26] H. G. Gallagher, J. N. Sherwood, and R. M. Vrcelj, Growth and dislocation studies of $\beta$-HMX, Chem. Cent. J. **8**, 75 (2014).
[27] H. G. Gallagher, J. C. Miller, D. B. Sheen, J. N. Sherwood, and R. M. Vrcelj, Mechanical properties of $\beta$-HMX, Chem. Cent. J. **9**, 22 (2015).
[28] A. Pereverzev, Molecular dynamics study of diffusionless phase transformations in HMX: B-HMX twinning and $\beta$-$\varepsilon$ phase transition, J. Appl. Phys. **134**, 125105 (2023).
[29] Q. Zhu, A. R. Oganov, C. W. Glass, and H. T. Stokes, Constrained evolutionary algorithm for structure prediction of molecular crystals: Methodology and applications, Acta Cryst. B **68**, 215 (2012).
[30] S. Plimpton, Fast parallel algorithms for short-range molecular dynamics, J. Comput. Phys. **117**, 1 (1995).
[31] E. J. Chan and M. A. Neumann, Evaluation of general and tailor made force fields via X-ray thermal diffuse scattering using molecular dynamics and Monte Carlo simulations of crystalline aspirin, J. Chem. Theory Comput. **14**, 2165 (2018).
[32] G. D. Smith and R. K. Bharadwaj, Quantum-chemistry-based force field for simulations of dimethylnitramine, J. Phys. Chem. B **103**, 705 (1999).
[33] N. Mathew and R. C. Picu, Molecular conformational stability in cyclotrimethylene trinitramine crystals, J. Chem. Phys. **135**, 024510 (2011).
[34] L. B. Munday, P. W. Chung, B. M. Rice, and S. D. Solares, Simulations of high-pressure phases in RDX, J. Phys. Chem. B **115**, 4378 (2011).
[35] A. G. Shtukenberg, C. T. Hu, Q. Zhu, M. U. Schmidt, W. Xu, M. Tan, and B. Kahr, The third ambient aspirin polymorph, Cryst. Growth Des. **17**, 3562 (2017).
[36] R. W. Molt, Jr., T. Watson, Jr., V. F. Lotrich, and R. J. Bartlett, RDX geometries, excited states, and revised energy ordering of conformers via MP2 and CCSD(T) methodologies: Insights into decomposition mechanism, J. Phys. Chem. A **115**, 884 (2011).
[37] See Supplemental Material at http://link.aps.org/supplemental/10.1103/7cdh-875w for additional benchmark calculations, convergence plots, and details of the softmutation, which includes Refs. [39–49].
[38] https://github.com/RC-up/Predicting-twin-boundaries-in-molecular-crystals-using-USPEX.
[39] S. Hunter, T. Sutinen, S. F. Parker, C. A. Morrison, D. M. Williamson, S. Thompson, P. J. Gould, and C. R. Pulham, Experimental and DFT-D studies of the molecular organic energetic material RDX, J. Phys. Chem. C **117**, 8062 (2013).
[40] J. L. Lyman, Y.-C. Liau, and H. V. Brand, Thermochemical functions for gas-phase, 1,3,5,7-tetranitro-1,3,5,7-tetraazacyclooctane (HMX), its condensed phases, and its larger reaction products, Combust. Flame **130**, 185 (2002).
[41] G. L. Perlovich, S. V. Kurkov, A. N. Kinchin, and A. Bauer-Brandl, Solvation and hydration characteristics of ibuprofen and acetylsalicylic acid, AAPS PharmSci. **6**, 22 (2004).
[42] A. R. R. P. Almeida, C. A. D. Sousa, L. M. N. B. F. Santos, and M. J. S. Monte, Thermodynamic properties of sublimation of the ortho and meta isomers of acetoxy and acetamido benzoic acids, J. Chem. Thermodyn. **86**, 6 (2015).
[43] C. Ouvrard and S. L. Price, Toward crystal structure prediction for conformationally flexible molecules: The headaches illustrated by aspirin, Cryst. Growth Des. **4**, 1119 (2004).
[44] F. Della Pia, B. X. Shi, V. Kapil, A. Zen, D. Alfè, and A. Michaelides, Accurate and efficient machine learning interatomic potentials for finite temperature modelling of molecular crystals, Chem. Sci. **16**, 11419 (2025).
[45] V. V. Zhurov, E. A. Zhurova, A. I. Stash, and A. A. Pinkerton, Importance of the consideration of anharmonic motion in charge-density studies: A comparison of variable-temperature studies on two explosives, RDX and HMX, Acta Cryst. A **67**, 160 (2011).
[46] E. A. Zhurova, V. V. Zhurov, and A. A. Pinkerton, Structure and bonding in $\beta$-HMX-characterization of a trans-annular N···N interaction, J. Am. Chem. Soc. **129**, 13887 (2007).
[47] Y. Kim, K. Machida, T. Taga, and K. Osaki, Structure redetermination and packing analysis of aspirin crystal, Chem. Pharm. Bull. **33**, 2641 (1985).
[48] A. O. Lyakhov, A. R. Oganov, and M. Valle, How to predict very large and complex crystal structures, Comput. Phys. Commun. **181**, 1623 (2010).
[49] K. Li, X. Wang, F. Zhang, and D. Xue, Electronegativity identification of novel superhard materials, Phys. Rev. Lett. **100**, 235504 (2008).